Nanoscale

RSC Publishing

PAPER

View Article Online
View Journal | View Issue

Cite this: *Nanoscale*, 2013, **5**, 12582

A dealloying process of core–shell Au@AuAg nanorods for porous nanorods with enhanced catalytic activity†

Xia Guo,[a] Wei Ye,[b] Hongyan Sun,[b] Qiao Zhang[a] and Jian Yang*[ab]

Received 14th August 2013
Accepted 2nd October 2013

DOI: 10.1039/c3nr04304e

www.rsc.org/nanoscale

One-dimensional porous metallic nanomaterials have attracted much attention due to their unique shape and hollow structure. Herein, the gold nanorods in a porous shell of an AuAg alloy are synthesized *via* a dealloying process of the core–shell Au@AuAg nanorods at room temperature. The formation of tiny pores in the shell results in the huge red-shift, sharp decrease and drastic broadening of longitudinal surface plasmon resonance absorption. The continuous removal of silver from the porous nanorods leads to the breakage of tiny pores and leaves a rough surface on the nanorods behind. The rough surface gradually becomes smooth in the subsequent dealloying process. The surface structures of these intermediates are correlated with their absorption spectra and catalytic activities for the catalytic reduction of *p*-nitrophenol. The porous nanorods show a higher catalytic efficiency than the gold nanorods, the core–shell nanorods and the rough nanorods. The results indicate that the dealloying of anisotropic bimetal nanomaterials not only provides an effective pathway to carve the structures on the nanoscale but also offers numerous opportunities to observe novel optical properties and enhanced catalysis performances.

Introduction

Noble metal nanomaterials have attracted much attention over the past decades due to their promising potential in heterogeneous catalysis, chemical/biological sensing, optoelectronic devices and disease therapy.[1–6] Since their performances in these fields strongly depend on the shape, structure and composition, a myriad of metallic nanostructures including nanorods, nanoplates, nanoboxes and nanocages have been synthesized. Compared with the solid metal nanostructures, the hollow ones are quite distinguishable, because of their large specific surface area, unique optical properties, high reactivity and atom economy.[1–6] For example, the hollow nanostructure of gold expands its absorption to the near-infrared region, which allows it to effectively absorb IR photons and heat surrounding media through the photothermal effect.[1–3] This temperature increase is developed as a powerful tool for disease therapy. The advantages of the hollow naonstructures of noble metals in catalysis are also in evidence.[5,6] Hollow Pt nanoparticles exhibited a much higher electrocatalytic activity than the solid ones in the oxidation reaction of methanol.[6]

Compared with spherical nanoshells, nanoboxes, and nanocages, one-dimensional porous metallic nanomaterials are studied to a much less extent.[7–12] The first example comes from Au/Ag alloy nanotubes synthesized by a galvanic replacement reaction with silver nanowires as sacrificed templates.[7] The combination of the galvanic replacement reaction with the electroless plating of silver could extend the capability of this method to fabricate multiwalled Au/Ag alloy nanotubes.[8,9] Later, the core–shell Au@Ag nanorods, not the pure silver nanowires, were used as templates for the galvanic replacement reaction, producing rod-like gold nanorattles where the gold nanorods were surrounded by a non-contacted shell of Au or AuAg.[10,11] The tiny modification around the gold nanorods could obviously alter their optical properties, even if the modification occurs to the shell non-contacted with the gold nanorods. Providing the porous shell directly contacts with the gold nanorods at the core, the interaction between them probably results in another different but interesting optical behaviour. However, such a gold nanorod directly coated with a porous shell has not been synthesized before, to the best of our knowledge.

Herein, the gold nanorods in a porous shell of an AuAg alloy are achieved in a high yield by a dealloying process of the core–shell Au@AuAg nanorods with $Fe(NO_3)_3$ as an etching agent. Differrent from the previous galvanic replacements, no deposition of a metal is involved in this reaction, facilitating the

[a]*School of Chemistry and Chemical Engineering, South China University of Technology, Guangzhou 510640, P. R. China. E-mail: yangjian@scut.edu.cn; Fax: +86-0531-88364489*

[b]*Key Laboratory of Colloid and Interface Chemistry, Ministry of Education, School of Chemistry and Chemical Engineering Shandong University, Jinan 250100, P. R. China*

† Electronic supplementary information (ESI) available: The average hydrodynamic radius during the etching reaction; EDS spectra and the catalysis stability of the porous nanorods; the UV-vis absorption spectra of the solution in which core–shell Au@AuAg (Au–Ag = 7.5 : 7.5) nanorods reacted with 100 μL of 10 mM $Fe(NO_3)_3$; the average sizes of the original gold nanorods, core–shell nanorods, porous nanorods, rough nanorods and relatively smooth nanorods; the molar ratios of Ag/Au in the core–shell nanorods, porous nanorods, rough nanorods and smooth nanorods. See DOI: 10.1039/c3nr04304e

control in shape and structure. Meanwhile, the core–shell Au@AuAg nanorods, rather than the core–shell Au@Ag nanorods, are used to assist the formation of the porous shell attached to the surface of the gold nanorods. These refinements make the dealloying process distinctive from the reported ones, which are supported by *ex situ* TEM images and *in situ* absorption spectra. The tiny but unique structural changes in the shell greatly alter the optical properties of the nanorods. The as-obtained intermediates during the dealloying process are tested as the catalysts for the reduction of *p*-nitrophenol to disclose the correlation between the surface structure and the catalytic activity.

Results and discussion

The core–shell Au@AuAg nanorods are prepared by a modified method previously used for core–shell Au@Ag nanorods. In order to guarantee the coreduction of $AgNO_3$ with $HAuCl_4$ by ascorbic acid, NaOH and gold nanorods are used in the protocol to enhance the reducing ability of ascorbic acid and induce the underpotential deposition (UPD) process between Au and Ag(I).[13–15] Therefore, the coreduction process of $AgNO_3$ and $HAuCl_4$ for the AuAg alloy could be realized, which has been confirmed by the EDS spectra and UV-vis absorption spectra. As shown in the EDS spectrum (Fig. S1†), the Ag signals could be easily resolved for the core–shell Au@AuAg nanorods, indicating the presence of silver in the nanorods. The longitudinal surface plasmon resonance (LSPR) peak of the core–shell Au@AuAg nanorods is located between those of the gold nanorods and the core–shell Au@Ag nanorods (Fig. S2†), suggesting the formation of an alloy shell similar to that in spherical AuAg nanoparticles.[16]

The dealloying process of the core–shell Au@AuAg nanorods for the porous nanorods is first followed by UV-vis absorption spectra, as shown in Fig. 1a. After the addition of $Fe(NO_3)_3$, the UV-vis absorption spectra present a series of changes in peak position, peak intensity and full width at half maximum (FWHM), particularly in the case of the LSPR absorption. According to the changes of these characteristic parameters, the whole reaction could be divided into several stages, as shown in Fig. 1b. At Stage I, the LSPR peak quickly shifts towards the red at the beginning of the reaction, along with the decrease of the peak intensity and the broadening of the peak width. The intensity decrease and width broadening of the LSPR peak are so great that the originally intense LSPR peak almost disappears from the absorption spectra. As a result of these changes, the solution becomes almost transparent, although both gold and silver nanomaterials are supposed to have a strong absorption in this region. It should be pointed out that these changes cannot be correlated with the aggregation of the nanorods in the solution, because DLS measurements do not show any apparent change in the particle size during the whole process (Fig. S3†). At Stage II, the LSPR peak still moves to the red, but its intensity slightly increases and its width gradually narrows. The changes of the LSPR peak are much smaller than those at Stage I. At Stage III, the LSPR peak shifts to the blue, increases its intensity and narrows its width. Finally, all these changes stop at the end of the reaction.

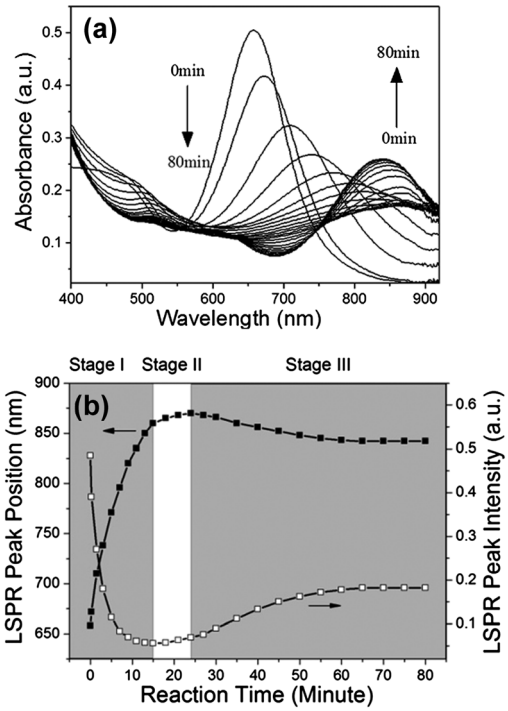

Fig. 1 (a) UV-vis absorption spectra of the solution at different times in which the core–shell Au@AuAg nanorods react with $Fe(NO_3)_3$. (b) Time evolutions of the peak intensity and peak position of the LSPR absorption during the dealloying process.

TEM is also employed to identify the composition and structure of the nanorods at different stages, which is then correlated with their optical properties to understand the above changes in the absorption spectra. The products at different stages of the dealloying process could be obtained by adding acetylacetone into the solution to stop the reaction, followed with the separation by centrifugation. The selection of acetylacetone as a reaction terminator is due to the huge difference in its coordinating ability with Fe(III) and Fe(II).[17] Acetylacetone strongly coordinates with Fe(III) ions, making the concentration of free Fe(III) in the solution greatly reduced. The coordinating ability of acetylacetone with Fe(II) is much weaker than that with Fe(III), indicating that more free Fe(II) ions would be left in the solution. So, the addition of acetylacetone into the reaction would remarkably reduce the molar ratio of free Fe(III)/Fe(II) in the solution, resulting in the decrease of the corresponding electrode potential. Then, the redox reaction between Ag and Fe(III) would be slowed down. The good solubility of the complexes between acetylacetone and Fe(III)/Fe(II) allows them to be easily separated from the product by centrifugation. The selection of a suitable reaction terminator like acetylacetone allows us to obtain the product at a desired stage for the subsequent characterization, which is very important to explain the complicate reaction process and obtain the interesting intermediates.

Fig. 2a and b show the TEM images of the original Au@AuAg core–shell nanorods. The core–shell nanorods display smooth

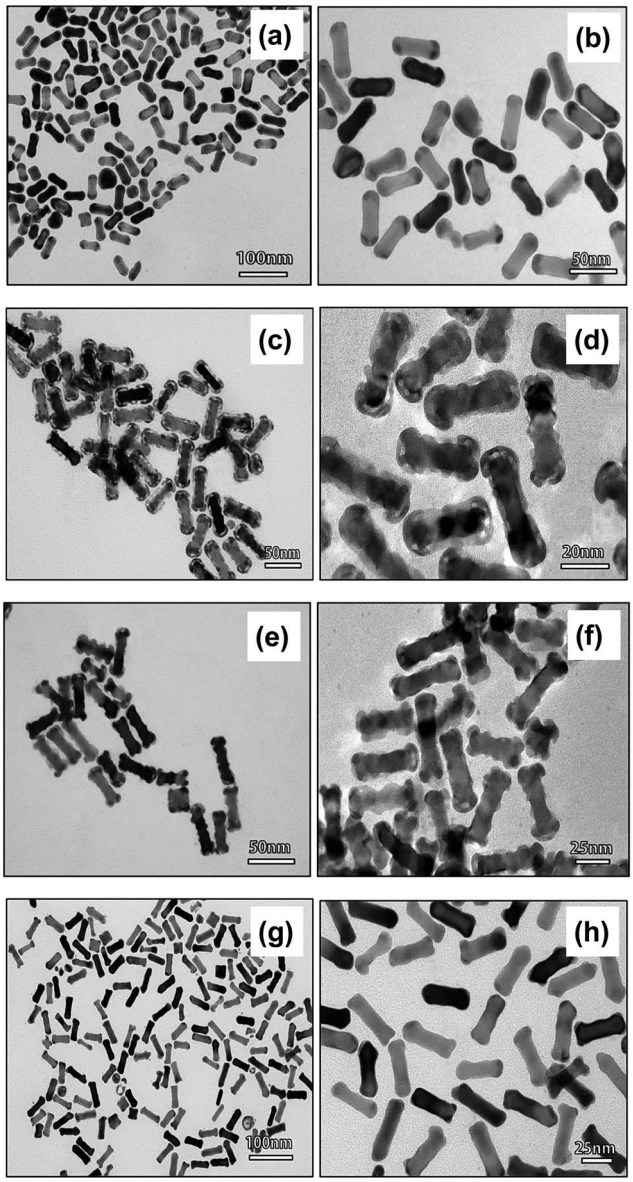

Fig. 2 TEM images of the original core–shell Au@AuAg nanorods (a and b) and the products obtained at the different stages of the dealloying process (c–h). (c and d) Stage I, (e and f) Stage II, (g and h) Stage III.

surfaces and uniform diameters from their body to their tip. The contrast difference at the tips of the core–shell nanorods could be attributed to the surface rearrangements or crystal defects caused by the silver growth.[18–20] The average length and diameter of the core–shell nanorods are much larger than those of the gold nanorods used as the core (Table S1†). This result validates the growth of a shell on the gold nanorods.

Fig. 2c and d show the TEM images of the product obtained at Stage I. The product still maintains the rod-like shape and similar size (Table S1†), but there are a number of significant contrast differences distributed at the periphery of the nanorods. The close-up observation indicates that the contrast differences might be caused by the tiny pores (2–3 nm) on/inside the shell of the core–shell nanorods. The formation of the pores could be assigned to the removal of elemental silver from the shell of the AuAg alloy, which has been confirmed by EDS spectra. As shown in Table S2,† the molar ratio of Ag/Au is reduced from 48 : 52 for the original core–shell Au@AuAg nanorods to 33 : 67 for these porous nanorods. The removal of silver from the AuAg alloy and the formation of the pores cause the LSPR peak to move toward the red more than 200 nm, decrease to ~1/10 of the previous intensity and become broader three times than before. All these distinctive changes could be correlated with the formation of a porous structure on the surface, which has been observed in the reports about nanoboxes, nanocages, nanoframes, *etc.*[1,21,22] However, there is a gold nanorod at the core in our case, which is supposed to have a strong absorption over this range. Because of the presence of the tiny pores in the shell, the intense LSPR absorption of the gold nanorods has been greatly weakened. Such a great decrease of the LSPR peak has not been reported in the gold nanorattles,[10–12] although they are also a combination of hollow structures and gold nanorods. This difference could be ascribed to the unique effect of a porous shell directly coated on the gold nanorods on the optical properties. In addition, the porous structure in the metallic nanoparticles allows them to become a good microcontainer for a variety of reactions or detections, which has been demonstrated in the later discussion.

Fig. 2e and f show the TEM images of the product at Stage II. Accompanied by the continuous removal of silver, the number of tiny pores around the nanorods is greatly reduced, leaving a rough surface behind. The changes in structure and composition make the LSPR peak of the nanorods red-shift slightly and a small increase at Stage II. A similar result was also reported for the rough gold nanorods obtained by a seed-assisted growth.[23] Compared with the gold nanorods as a seed, the rough nanorods also presented a much weaker LSPR peak.

Fig. 2g and h show the TEM images of the product at Stage III. The product is composed of a large number of the nanorods with a remarkably reduced size (Table S1†) and a relatively smooth surface. Both of them could be attributed to the removal of silver from the nanorods. This surface smoothing is also reflected in the absorption spectra as the obvious blue-shift and intensity increase of the LSPR peak, all of which are not reported before for the dealloying process. The correlation between the surface smoothing and the above changes in the absorption spectra has been documented in the literature.[24–26] Lee and Xie reported a template-free method for high-quality gold nanoflowers.[24] The absorption spectra of the gold nanoflowers were recorded and compared with those of the nearly spherical gold nanoparticles in a comparable size. It was found that the SPR peak of the nearly spherical gold nanoparticles showed an obvious blue-shift in comparison with that of gold nanoflowers, indicating the correlation between the smooth surface of the nanoparticles and the blue-shift of the SPR peak. Sau and Rogach developed a high-yield approach for multi-spiked gold nanoparticles without the usage of seeds.[26] As the concentration of Ag(I) increased or that of ascorbic acid decreased, the number and size of the spikes would decrease, which can be regarded as a sort of the surface smoothing. This structure change also leads to the blue-shift and intensity increase of the SPR peak, consistent with our results.

Based on the above results from TEM and UV-vis absorption spectroscopy, Scheme 1 elucidates the dealloying process of the core–shell Au@AuAg nanorods. At the beginning of this process, Ag in the AuAg alloy shell is etched away by Fe(III), resulting in the formation of tiny pores in the shell of nanorods. As a result, the coupling between the SPRs from the inner and outer surface of the tiny pores would induce the huge red-shift and sharp decrease of the LSPR peak in the absorption spectra,[27] as observed in Stage I. The removal of silver also makes some contributions to these changes. As the etching reaction proceeds further, the continuous removal of silver from the porous shell leads to the breakage of the pores in the shell and then the formation of a rough surface. These subtle changes in composition and structure are reflected as the slight red-shift and small increase of the LSPR peak, as presented in Stage II. At the end of the dealloying process, silver is almost removed from the shell, producing the nanorods with a relatively smooth surface. This surface smoothing reduces the number and sharpness of the spikes on the surface, and makes the LSPR peak blue-shifted and enhanced, as shown in Stage III.

Since UV-vis absorption spectroscopy is highly sensitive to the composition and structure of metallic nanoparticles, the temporal evolution of the LSPR absorption is monitored to clarify the effects of different reagents on the dealloying process. Fig. 3a shows the temporal evolution of the LSPR absorption of the core–shell Au@AuAg nanorods treated with different amounts of $Fe(NO_3)_3$. The changes of the LSPR absorption in peak position and peak intensity obviously speed up with the increase of $Fe(NO_3)_3$. This result could be assigned to the oxidizing role of Fe(III) in the etching reaction. The increase of Fe(III) would accelerate the removal of silver and then promote the dealloying process. It is noticed that the LSPR absorption during the dealloying process exhibits almost the same maximal peak position and the minimal peak intensity, although different amounts of Fe(III) are involved. This result indicates that the increase of $Fe(NO_3)_3$ does not change the related intermediates, but simply increases the evolution speed.

Fig. 3b shows the temporal evolution of the LSPR absorption from the core–shell Au@AuAg nanorods with the shell at different ratios of Ag/Au treated with $Fe(NO_3)_3$. The total molar number of $AgNO_3$ and $HAuCl_4$ for the shell growth is kept as the same to make sure that the shells at different molar ratios of Ag/Au have thicknesses close to each other. The LSPR peak of the core–shell Au@AuAg nanorods prepared with a molar ratio of $AgNO_3/HAuCl_4$ at 12/3 exhibits a minimal intensity close to that prepared with a molar ratio at 10/5. But there is an apparent difference between the two nanorods in the red-shift of the LSPR peak. These results indicate that the porous nanorods produced by the dealloying process are closely related to the molar ratio of Ag/Au in the alloy shell. The molar ratio of Ag/Au in the alloy also affects the product obtained at the end of the dealloying process, due to different amounts of Au left from the alloy shell. When the molar ratio of $AgNO_3/HAuCl_4$ is 7.5/7.5 for the growth of the alloy shell, the absorption spectra do not show apparent changes, indicating that the removal of silver is inhibited (Fig. S4†). A similar result is also observed in the dealloying process of Au/Ag alloys with HNO_3, although the exact mechanism is still obscure.[28] In that report, elemental silver could be completely removed by HNO_3 from Au/Ag alloys with the content of Au less than 54%. But no apparent lose of Ag was observed from the Au/Ag alloys, when the content of Au was above 54%.

Fig. 3c shows the temporal evolution of the LSPR peak of the core–shell Au@AuAg nanorods with the shells of different thicknesses treated with $Fe(NO_3)_3$. The shells of different thicknesses are obtained by using different amounts of $AgNO_3$ and $HAuCl_4$ in a fixed ratio for the shell growth. The LSPR peaks of these nanorods display similar changes in terms of the peak position and the peak intensity, but differ a lot in the specific data. The results indicate that the porous nanorods corresponding to these changes are strongly affected by the shell thickness. Furthermore, the extents of the red-shift and intensity decrease of the LSPR peak are reduced with the decrease of the shell thickness. As aforesaid, the final product at the end of the dealloying process is closely connected with the remnant Au in the alloy shell. Thus, the LSPR peak from the core–shell nanorods with the shells of different thicknesses stops at different positions.

The presence of CTAB in the solution plays an important role in the dealloying process of the core–shell Au@AuAg nanorods, because it stabilizes the nanorods, lowers the electrode potential of Ag(I)/Ag and then promotes the dealloying process. The facts make the studies about the effect of CTAB on the dealloying process necessary. Fig. 3d shows the temporal evolution of the LSPR peak of the core–shell Au@AuAg nanorods etched by $Fe(NO_3)_3$ at different concentrations of CTAB. In the course of the dealloying process, the LSPR peaks of the core–shell nanorods treated at different concentrations of CTAB display similar maximal peak positions and minimal peak intensities, indicating the alike intermediates in the reaction. But the higher concentration of CTAB induces a faster change of the LSPR peak. This result could be ascribed to the accelerated oxidation of silver, due to the presence of Br^- in the reaction. Meanwhile, it is noticed that the LSPR peak of the core–shell nanorods treated at a high concentration of CTAB stops at a shorter wavelength at the end of this dealloying process,

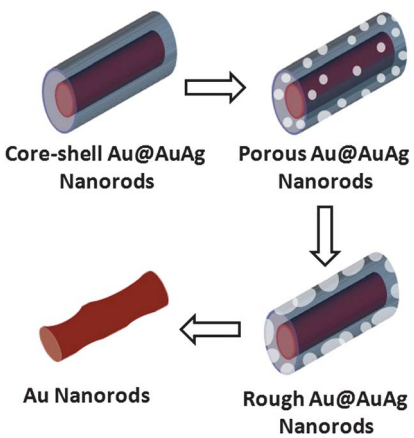

Scheme 1 Schematic illustration of the dealloying process of core–shell Au@AuAg nanorods induced by $Fe(NO_3)_3$.

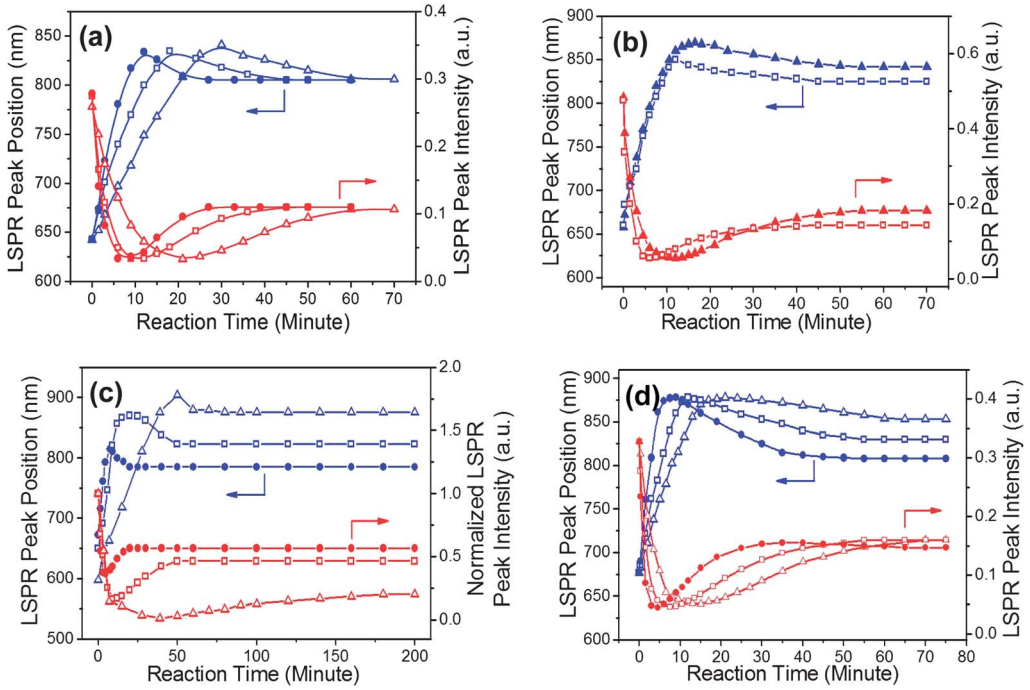

Fig. 3 (a) The effect of Fe(III) on the temporal evolution of the LSPR peak. The concentration of $Fe(NO_3)_3$ is fixed at 10 mM, but their volume varies. Hollow triangles: 80 μL; hollow squares: 100 μL; solid dots: 120 μL. (b) The effect of the molar ratios of Au/Ag in the shell on the temporal evolution of the LSPR peak. The total number of $HAuCl_4$ and $Ag(NO_3)_3$ for the shell is kept as the same. Solid triangles: $Ag(NO_3)_3/HAuCl_4 = 10/5$; hollow squares: $Ag(NO_3)_3/HAuCl_4 = 12/3$. (c) The effect of the shell thicknesses on the temporal evolution of the LSPR peak. Different amounts of $AgNO_3$ and $HAuCl_4$ in a fixed ratio are used for the shell growth. Solid dots: 60 μL 4 mM $AgNO_3$ and 12 μL 10 mM $HAuCl_4$; hollow squares: 120 μL 4 mM $AgNO_3$ and 24 μL 10 mM $HAuCl_4$; hollow triangles: 240 μL 4 mM $AgNO_3$ and 48 μL 10 mM $HAuCl_4$. (d) The effect of CTAB on the temporal evolution of the LSPR peak. Hollow triangles: 0.5 mM CTAB; hollow squares: 2.5 mM CTAB; solid dots: 5.0 mM CTAB.

although all of them present similar peak intensities. The results might be attributed to the differences caused by different concentrations of CTAB in surface smoothing, because the high concentration of CTAB would benefit the surface smoothing of gold nanoparticles *via* Ostwald-ripening. Otherwise, the rough surface might be less changed. A similar phenomenon was also reported in the reshaping of gold nanostars into spherical particles by CTAB.[29] As the concentration of CTAB increased, this reshaping became faster.

The surface structure on the nanorods, such as a porous shell, as well as a rough surface, not only alters their optical properties, but also enhances their catalytic activity due to the greatly increased surface area. This result could be demonstrated by using the catalytic reduction of *p*-nitrophenol as a model, because this reducing reaction could be catalyzed by many metallic nanoparticles including gold and silver.[10,30,31] At the same time, the product of this reducing reaction, aminophenol, is a valuable intermediate for many analgesic and antipyretic drugs, such as paracetamol, phenacetin, and so on. Fig. 4a shows the typical UV-vis absorption spectra, during the reduction of *p*-nitrophenol by $NaBH_4$ with the gold nanorods as a catalyst. As the catalytic reaction proceeds, the absorption peak at 400 nm originating from *p*-nitrophenol gradually decreases, indicating the continuous reduction of *p*-nitrophenol. Meanwhile, the absorbance at 300 nm related to aminophenol slightly increases and leads to a small peak there. The results are in good agreement with the reported reduction of *p*-nitrophenol to aminophenol.[32] As shown in Fig. 4b, the reducing reaction would stop in the absence of the catalyst or the reducing agent (not shown here), confirming that both of

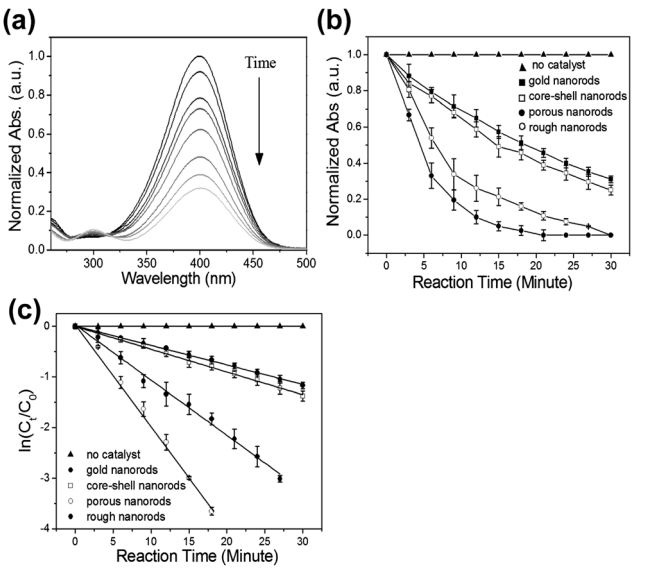

Fig. 4 (a) The temporal development of the absorption spectra of *p*-nitrophenol reduced by $NaBH_4$ with the gold nanorods as a catalyst. (b) The evolution of the absorbance of *p*-nitrophenol at 400 nm with different nanorods as the catalyst. (c) The dependence of $\ln(C_t/C_0)$ obtained from different nanorods with the reaction time.

them are indispensable for the reaction. After 15 min, ~95% of *p*-nitrophenol has been reduced in the presence of the porous nanorods. This conversion efficiency is much higher than those obtained from the other catalysts, such as 42% for the gold nanorods, 51% for the core–shell Au@AuAg nanorods, and 79% for the rough Au@AuAg nanorods. The result could be substantially attributed to the large specific surface area of the porous nanorods and/or their abundant surface defects caused by the dealloying process. The surface defects like steps, kinks and dislocations are usually low coordinated, and then highly active for the catalysis.[33–35] Although there is a difference in the molar ratio of Ag/Au for different nanorods, this effect on the catalytic performance is quite small,[36,37] which is also supported by the comparison between the gold nanorods and the core–shell Au@AuAg nanorods.

In order to give a quantitative description about the catalytic performance, the apparent rate constants of the reducing reaction are calculated. Since $NaBH_4$ is far excessive for the reduction of *p*-nitrophenol, it is reasonable to regard the concentration of $NaBH_4$ as a constant throughout the reaction. In this context, the pseudo-first-order kinetics could be applied to achieve the apparent rate constant. As shown in Fig. 4c, $\ln(C_t/C_0)$ exhibits a linear relationship with the reaction time. The apparent rate constants of the gold nanorods, core–shell Au@AgAu nanorods, porous Au@AgAu nanorods, and rough Au@AuAg nanorods are 0.0385, 0.0450, 0.206, and 0.109 min^{-1}, respectively. The result confirms the high catalytic activity of the porous Au@AuAg nanorods again. The structural stability of the porous Au@AuAg nanorods is directly assured by TEM images and the cyclic test. The catalytic activity of the porous nanorods is maintained after three runs (Fig. S5†), indicating a good stability of the porous Au@AuAg nanorods in the reducing reaction of *p*-nitrophenol.

Conclusions

In summary, the dealloying process limited in the alloy shell of core–shell one-dimensional nanomaterials has been achieved by the core–shell Au@AuAg nanorods etched with $Fe(NO_3)_3$. Using acetylacetone as a reaction terminator enables us to obtain the high-quality intermediates during the dealloying process. TEM images reveal that the core–shell nanorods turn to the nanorods with a large number of tiny pores in the alloy shell at the beginning of the dealloying process. Then, the tiny pores gradually break, leading to a rough surface for the nanorods. Finally, the rough nanorods become relatively smooth, probably due to the Ostwald-ripening process. The porous nanorods are particularly interesting not only in the structure but also in the absorption. The LSPR peak of the porous nanorods exhibits a huge red-shift and a great decrease, although the solid gold nanorods at the core are supposed to give a strong absorbance over this range. The large surface area and the abundant surface defects caused by the dealloying process probably enable the porous nanorods to become a potential candidate for catalysis, which has been demonstrated with the reduction of *p*-nitrophenol as a model. The porous nanorods present higher conversion efficiency than the gold nanorods, the core–shell nanorods and the rough nanorods in the catalysis.

Experimental section

Chemicals and instruments

$HAuCl_4 \cdot xH_2O$ (x = 3–5, Au ~ 47.8%) was obtained from July Chemical Co. Ltd in Shanghai. Cetyltrimethylammonium bromide (CTAB, ≥99%) and polyvinylpyrrolidone K30 (PVP K30) were obtained from Bio-Life Sci & Tech. Co. Ltd also in Shanghai. Ethanol (≥99.7%), NaOH (≥96.0%), sodium borohydride (≥96%), ascorbic acid (AA, ≥99.7%), acetylacetone (≥99.0%) and *p*-nitrophenol (≥99.5%) were purchased from Sinopharm Chemical Reagent Co. Ltd also in Shanghai. Iron(III) nitrate nonahydrate (≥98.5%) and silver nitrate (≥99.8%) were ordered from Kermel Chemical Reagent Co. Ltd in Tianjin. All these reagents were used without any further purification.

UV-vis absorption spectra were recorded in the range of 400–950 nm at room temperature using a Shimadzu UV-2450 spectrophotometer. Low-magnification TEM images were acquired with a JEM-1011 transmission electron microscope at an accelerating voltage of 100 kV. EDS spectra were obtained on a JEOL 2100 analytical transmission electron microscope equipped with an energy dispersive X-ray spectrometer (EDS). The intermediates for TEM analysis were obtained by adding diluted acetylacetone into the solution and then centrifuging to remove the excess of the reactants and surfactants. Afterwards, the deposit was dispersed in distilled water, and dropped on a copper grid coated with an amorphous carbon film. The average hydrodynamic size during the etching course was measured using a DAWN HELEOS made in America.

Synthesis of core–shell Au@AuAg nanorods

The high-quality gold nanorods were obtained *via* a typical seed-mediated growth process.[38,39] Then, the as-obtained gold nanorods were purified by centrifugation twice at 10 000 rpm for 10 min and then dispersed in 0.1 M CTAB. The preparation of the core–shell Au@AuAg nanorods was developed from the method for core–shell Au@Ag nanorods.[13] In brief, 2 mL of the gold nanorod solution, 120 μL of 4 mM $AgNO_3$ and 24 μL of 10 mM $HAuCl_4$ were added into 10 mL of 1 wt% PVP. After the solution was heated to 40 °C, 0.426 mL of 78.8 mM AA and 0.75 mL of 0.1 M NaOH were added. As a result, the color of the solution gradually turned from wine red to green within a few minutes. The solution was cooled down 30 minutes later. Finally, the core–shell Au@AuAg nanorods were collected from the solution by centrifugation and dispersed into 8 mL of 0.5 mM CTAB for later use.

Chemical etching of core–shell Au@AuAg nanorods

100 μL of 10 mM fresh $Fe(NO_3)_3$ was added into 2 mL of the core–shell Au@AuAg nanorods in the presence of 0.5 mM CTAB at room temperature. The UV-vis absorption spectrum of the solution was tracked at a regular interval to follow the change of the optical properties of the nanorods. The reaction can be stopped by adding an appropriate amount of acetylacetone.

Catalytic reduction of *p*-nitrophenol

The catalytic reduction of *p*-nitrophenol was conducted according to a reported procedure.[30] 9 mL of 0.925×10^{-4} M *p*-nitrophenol was added to 1 mL of 0.3 M ice-cold $NaBH_4$ aqueous solution, and the solution was stirred for 10 min at room temperature. The different nanorods (Au nanorods, core–shell Au@AuAg nanorods, porous Au@AuAg gold nanorods, or rough Au@AuAg gold nanorods) were added into the above solution. The numbers of the different nanorods were kept as almost the same, because they were obtained from the same batch of the gold nanorods. The catalytic reduction of *p*-nitrophenol was monitored by the absorption spectra of the solution at a regular interval.

Acknowledgements

This work is supported by Natural Science Foundation of China (no. 21071055, and 51172076), New Century Excellent Talents in University (NCET-10-0369), New Faculty Start-up funding in Shandong University, Independent Innovation Foundations of Shandong University (2012ZD007), and Shandong Provincial Natural Science Foundation for Distinguished Young Scholar (JQ201205). We also would like to thank Prof. Jinhua Zhan for the use of some facilities in his lab.

Notes and references

1 J. Chen, B. Wiley, Z.-Y. Li, D. Campbell, F. Saeki, H. Cang, L. Au, J. Lee, X. D. Li and Y. Xia, *Adv. Mater.*, 2005, **17**, 2255.
2 Y. Xia, W. Y. Li, C. M. Cobley, J. Chen, X. Xia, Q. Zhang, M. X. Yang, E. C. Cho and P. K. Brown, *Acc. Chem. Res.*, 2011, **44**, 914.
3 L. Gao, J. Fei, J. Zhao, H. Li, Y. Cui and J. Li, *ACS Nano*, 2012, **6**, 8030.
4 H. Liu, J. Qu, Y. Chen, J. Li, F. Ye, J. Y. Lee and J. Yang, *J. Am. Chem. Soc.*, 2012, **134**, 11602.
5 J. W. Hong, S. W. Kang, B.-S. Choi, D. Kim, S. B. Lee and S. W. Han, *ACS Nano*, 2012, **6**, 2410.
6 H. P. Liang, H. M. Zhang, J. S. Hu, Y. G. Guo, L. J. Wan and C. L. Bai, *Angew. Chem., Int. Ed.*, 2004, **43**, 1540.
7 Y. Sun, B. T. Mayers and Y. Xai, *Nano Lett.*, 2002, **2**, 481.
8 Y. Sun and Y. Xia, *Adv. Mater.*, 2004, **16**, 264.
9 Y. Sun, B. Wiley, Z.-Y. Li and Y. Xia, *J. Am. Chem. Soc.*, 2004, **126**, 9399.
10 Y. Khalavka, J. Becker and C. Sönnichsen, *J. Am. Chem. Soc.*, 2009, **131**, 1871.
11 K. W. Hu, T. M. Liu, K. Y. Chung, K. S. Huang, C. T. Hsieh, C. K. Sun and C. S. Yeh, *J. Am. Chem. Soc.*, 2009, **131**, 14186.
12 E. C. Cho, P. H. C. Camargo and Y. N. Xia, *Adv. Mater.*, 2010, **22**, 744.
13 M. Z. Liu and P. Guyot-Sionnest, *J. Phys. Chem. B*, 2004, **108**, 5882.
14 N. G. Tognalli, E. Cortés, A. D. Hernández-Nieves, P. Carro, G. Usaj, C. A. Balseiro, M. E. Vela, R. C. Salvarezza and A. Fain-stein, *ACS Nano*, 2011, **5**, 5433.
15 T. Guo and Y. Tan, *Nanoscale*, 2013, **5**, 561–569.
16 C. Wang, H. Yin, R. Chan, S. Peng, S. Dai and S. Sun, *Chem. Mater.*, 2009, **21**, 433.
17 J. A. Dean, *J. A. Lange's Handbook of Chemistry*, McGraw-Hill, Inc, New York, 15 edn, 1999, ch. 8, p. 88.
18 M. Z. Liu and P. Guyot-Sionnest, *J. Phys. Chem. B*, 2004, **108**, 5882–5888.
19 C. S. Ah, S. D. Hong and D. J. Jang, *J. Phys. Chem. B*, 2001, **105**, 7871–7873.
20 M. F. Cardinal, B. Rodriguez-Gonzalez, R. A. Alvarez-Puebla, J. Perez-Juste and L. M. Liz-Marzan, *J. Phys. Chem. C*, 2010, **114**, 10417–10423.
21 X. Lu, L. Au, J. McLellan, Z.-Y. Li, M. Marquez and Y. Xia, *Nano Lett.*, 2007, **7**, 1764.
22 Q. Zhang, C. M. Cobley, J. Zeng, L. P. Wen, J. Y. Chen and Y. N. Xia, *J. Phys. Chem. C*, 2010, **114**, 6396.
23 P. Aldeanueva-Potel, E. Carbó-Argibay, N. Pazos Perez, S. Barbosa, I. Pastoriza-Santos, R. A. Alvarez-Puebla and L. M. Liz Marzan, *ChemPhysChem*, 2012, **13**, 2561.
24 J. Xie, Q. Zhang, J. Y. Lee and D. I. C. Wang, *ACS Nano*, 2008, **2**, 2473.
25 S. Trigari, A. Rindi, G. Margheri, S. Sottini, G. Dellepiane and E. Giorgetti, *J. Mater. Chem.*, 2011, **21**, 6531.
26 T. K. Sau, A. L. Rogach, M. Döblinger and J. Feldmann, *Small*, 2011, **7**, 2188.
27 E. Prodan, C. Radloff, N. J. Halas and P. Nordlander, *Science*, 2003, **302**, 419.
28 L. Martinez, M. Segarra, M. Fernandez and F. Espiell, *Metall. Trans. B*, 1993, **24**, 827.
29 L. Rodríguez-Lorenzo, J. M. Romo-Herrera, J. Pérez-Juste, R. A. Alvarez-Puebla and L. M. Liz-Marzán, *J. Mater. Chem.*, 2011, **21**, 11544.
30 X. Guo, Q. Zhang, Y. Sun, Q. Zhao and J. Yang, *ACS Nano*, 2012, **6**, 1165.
31 H. Wu, P. Wang, H. He and Y. Jin, *Nano Res.*, 2012, **5**, 135.
32 S. Kundu, S. Lau and H. Liang, *J. Phys. Chem. C*, 2009, **113**, 5150.
33 J. Lee, J. C. Park and H. Song, *Adv. Mater.*, 2008, **20**, 1523.
34 S. He, C. Li, H. Chen, D. Su, B. Zhang, X. Cao, B. Wang, M. Wei, D. G. Evans and X. Duan, *Chem. Mater.*, 2013, **25**, 1040.
35 L. Zhang and C. Zhang, *Nanoscale*, 2013, **5**, 5794.
36 Y. Sun and C. Lei, *Angew. Chem., Int. Ed*, 2009, **48**, 6824.
37 H. Wu, P. Wang and Y. Jin, *Nano Res.*, 2012, **5**, 135.
38 B. Nikoobakht and M. C. El-sayed, *Chem. Mater.*, 2003, **15**, 1957.
39 T. K. Sau and C. J. Murphy, *Langmuir*, 2004, **20**, 6414.

